Analyst

ROYAL SOCIETY OF CHEMISTRY

PAPER

Cite this: *Analyst*, 2021, **146**, 714

A rolling circle amplification based platform for ultrasensitive detection of heparin

Lei Lin,†[a] Bingzhi Li,†[b] Xiaorui Han,[c] Fuming Zhang,[c] Xing Zhang *[b] and Robert J. Linhardt *[c]

Received 16th October 2020,
Accepted 13th November 2020

DOI: 10.1039/d0an02061c

rsc.li/analyst

Heparin has a variety of pharmacological uses, including applications for anti-tumor metastasis, anti-inflammatory and anti-viral activities and is widely used as a clinical anticoagulant. Due to its widespread applications in the clinical procedures, monitoring heparin levels is critically important to ensure the safe use of heparin and to prevent overdose and complications, such as hemorrhage and thrombocytopenia. However, traditional heparin detection relies on the measurements of the activated clotting time or activated partial thromboplastin time, which are not sufficiently reliable or accurate measurements for certain clinical settings. In this work, we describe a dumbbell probe-aided strategy for ultrasensitive and isothermal detection of heparin based on a uniquely strong protamine–heparin interaction and rolling circle amplification driven signal amplification. The detection limit for heparin is 12.5 ng mL^{-1} (0.83 nM), which is much lower than the therapeutic level of heparin in cardiovascular surgery (17–67 μM) and in post-operative and long-term treatment (1.7–10 μM). Additionally, the proposed sensing platform works well for heparin monitoring in human plasma samples. This simple and ultrasensitive heparin biosensor has potential application in diagnostics, therapeutics, and in biological research.

Introduction

Heparin is a naturally occurring sulfated polysaccharide, playing a vital role in various physiological and pathophysiological processes such as venous thromboembolism, lipid transport and metabolism, cell growth, cell differentiation, and blood anticoagulation.[1–4] Consequently, it is used in a variety of pharmacological applications, including anti-tumor metastasis,[5] anti-inflammatory[6] and anti-viral activities,[7] regulating plasma lipids,[8] and is a widely used clinical anticoagulant.[2] Due to its widespread applications in clinical procedures, particularly during cardiac/vascular surgery and kidney dialysis, monitoring heparin levels is critically important for the safe use of heparin, in preventing overdose and alleviating complications, such as hemorrhage and thrombocytopenia.[9–11] In the clinical use of heparin as an anticoagulant, the therapeutic dosing level is 2–8 U mL^{-1} (17–67 μM) in cardiovascular surgery and 0.2–1.2 U mL^{-1} (1.7–10 μM) in postoperative and long-term care.[12] Thus, it is important to develop simple and ideally real-time and continuous measurements of heparin levels in serum during such surgery and postoperative therapy. In addition, there is also a need for detection methods that can monitor the levels of heparin within infusion solutions to avoid dangerous human errors in dosing, especially in pediatric patients.

Traditional heparin detection methods in clinical procedures rely on the measurement of the activated clotting time (ACT) or activated partial thromboplastin time (aPPT).[13,14] These methods are not sufficiently reliable or accurate in many clinical settings due to their lack of specificity and potential interference circulating substances.[15] Other methods, relying on electrochemistry,[16–18] nuclear magnetic resonance spectrometry,[19] and liquid chromatography-mass spectrometry,[20] have been proposed for heparin analysis. Nevertheless, these suffer from the drawbacks such as time-consuming process, complicated procedures, and, thus, are limited for clinical applications. Developing new methods for heparin detection, especially its ultrasensitive detection is important, not only to facilitate clinical studies, but also improve our understanding of the role of heparin in the critical biological processes. However, the ultrasensitive analysis of heparin is incredibly challenging due to its low concentrations in complex biological mixtures and the chemical complexity of its glycan chains.[21–23] Furthermore, heparin not only lacks natural chromophores and fluorophores,[24] but there are no specific

[a]*School of Environment, Nanjing Normal University, Wenyuan Road 1, Nanjing 210023, China*
[b]*School of Food Science and Pharmaceutical Engineering, Nanjing Normal University, Wenyuan Road 1, Nanjing 210023, China.*
E-mail: zhangxing@njnu.edu.cn
[c]*Department of Chemistry and Chemical Biology, Center for Biotechnology and Interdisciplinary Studies, Rensselaer Polytechnic Institute, 110 8th Avenue, Troy, New York 12180, USA. E-mail: linhar@rpi.edu*
†These authors contributed equally.

antibodies that can recognize heparin and there are no methods for signal amplification, further increasing the difficulty of ultrasensitive heparin detection.

Rolling circle amplification (RCA) is an isothermal enzymatic process that utilizes unique polymerases to amplify a short DNA or RNA primer to form a long single stranded DNA or RNA with tens to hundreds of tandem repeats.[25,26] RCA can be conducted at a constant temperature (room temperature to 37 °C) in solution, on a solid support or even in a complex biological environment.[27] The ability of RCA to grow a long DNA chain on a solid support or inside a cell from one molecular binding event enables detection of targets at the single molecule level. This simple and powerful technique has been extensively used to develop sensitive diagnostic methods for nucleic acids, small molecules, proteins, and cells.[28] However, despite its superb properties, the RCA based platform has not been applied to heparin detection.

In this work, we describe a dumbbell probe-aided strategy for ultrasensitive and isothermal detection of heparin on the basis of the uniquely strong protamine–heparin interaction and RCA-driven efficient signal amplification. The basic principle relies on the competitive affinity behavior of heparin and single-stranded DNA on positively charged protamine. In the absence of heparin, protamine effectively blocks the RCA reaction through forming a tightly bound protamine–DNA complex. Nevertheless, when heparin is introduced and competes with a DNA primer, the blocking effect disappears due to the stronger affinity of the heparin–protamine interaction. The release of primer promptly triggers RCA generating a strong fluorescent readout, offering a high signal-to-background ratio. Owing to the high amplification efficiency of RCA, the sensing system proposed provides an excellent isothermal heparin-screening platform with wide linear range and low limit of detection. Moreover, because of the dumbbell-shaped structure, the sealed probe is not activated by small amounts of random nucleic acids present in the sample suggesting that the specificity of heparin recognition can be remarkably enhanced. This simple and ultrasensitive heparin biosensor has potential uses in diagnostics, therapeutics and biological research.

Experimental section

Materials

Oligonucleotides were purchased from Integrated DNA Technologies, Inc. (Coralville, US). Sequences of oligonucleotide probes used in this work are listed as follows: dumbbell template precursor, 5′-Phos-TCG GAC AAC TGT AGA AAG AGC TGC GCG CAC TGT CCG ACC GAA TCC CTA ACC CGC CCT ATC CCA AAC ATG GAT TCG G-3′; t-DNA, 5′-TTT GGG ATA GGG CGG GTT AGG GAT T-3′. T4 DNA ligase, Exonuclease I, Exonuclease III, phi29 DNA polymerase, 10× T4 DNA ligase reaction buffer (400 mM Tris-HCl, 100 mM $MgCl_2$, 100 mM dithiothreitol, 5 mM ATP, pH 7.8 at 25 °C), 10× phi29 DNA polymerase reaction buffer (500 mM Tris-HCl, pH 7.5 at 25 °C, 100 mM $MgCl_2$, 100 mM $(NH_4)_2SO_4$, 40 mM dithiothreitol), deoxyribonucleotides mixture (dNTPs), and nuclease-free water were bought from Thermo Fisher Scientific Inc. (Waltham, US). Protamine sulfate, SYBR® Green I nucleic acid gel stain (10 000× in DMSO), heparin and heparan sulfate were purchased from Sigma-Aldrich (St Louis, US). Other regents of analytical grade were obtained from VWR International, LLC. (Radnor, US) and used without further purification.

Preparation and electrophoresis analysis of the dumbbell template

The dumbbell template was prepared from 5′-phosphorylated dumbbell template precursor using self-templated ligation catalyzed by T4 DNA ligase. The ligation reaction was conducted in a 100 μL of reaction mixture containing 10 μL of dumbbell template precursor (10 μM), 10 μL of 10× T4 DNA ligase reaction buffer, 70 μL of nuclease-free H_2O, and 10 μL of T4 DNA ligase (5 Weiss U μL^{-1}). After the incubation at 37 °C for 60 min, the reaction mixture was then heated at 65 °C for 10 min to terminate the ligation process, followed by the addition of exonuclease I (20 U μL^{-1}) and exonuclease III (200 U μL^{-1}) to digest residual DNA. The enzymes were denatured by heating the reaction mixture at 80 °C for 20 min. The dumbbell template prepared was stored at −20 °C before use. Denaturing polyacrylamide gel (20%) electrophoresis (PAGE) was used to characterize both the non-ligated dumbbell template precursor and the dumbbell template. Electrophoresis was performed at 450 V for 45 min. The gel was then stained with SYBR Green I and visualized using a Bio-Rad gel system (Hercules, US) (Fig. 2A).

RCA reaction and fluorescence measurement

In a typical RCA reaction, 2 μL of i-DNA (100 nM), 1 μL of protamine (0.1 μg mL^{-1}), 0.5 μL of 10× phi29 DNA polymerase reaction buffer, 0.5 μL of dNTP (10 mM for each of dATP, dGTP, dCTP and dTTP), water and varying amounts of heparin were mixed well and incubated at room temperature for 10 min, followed by the addition of 2 μL of the prepared dumbbell template (100 nM) and 2 μL of phi29 DNA polymerase (0.5 U μL^{-1}). After the incubation at 37 °C for 1 h, the mixture was mixed with 2 μL 50× Sybr Green I and measured at 520 nm with the excitation of 497 nm *via* Synergy Multi-Mode Reader (BioTek, US). Whole blood solutions (obtained from three healthy adults) were centrifuged at 3500 rpm for 10 min under room temperature to collect plasma samples. Heparin standard solutions were then spiked in the yielded plasma samples with the final concentrations of 40, 60, and 80 μg mL^{-1}, respectively. All the other experimental conditions are the same as the description mentioned above. All the tests were performed in triplicate.

Results and discussion

Strategy for T4 polynucleotide kinase (PNK) activity detection

A schematic for heparin detection is shown in Fig. 1. Protamine is a low molecular weight (*ca.* 4500 Da) nuclear

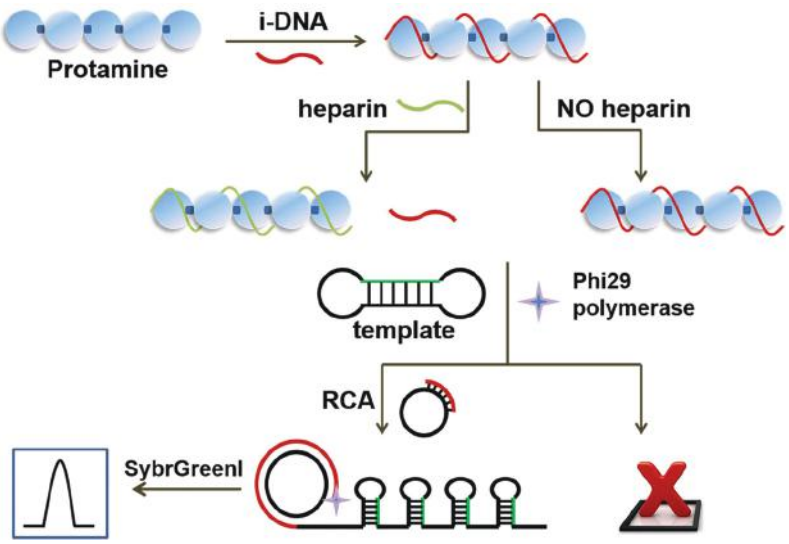

Fig. 1 Schematic representation of rolling circle amplification based platform for ultrasensitive detection and quantification of heparin. The red strand is single-stranded DNA, and green strand is heparin.

protein having 20 positive charges under physiological conditions due to its arginine rich sequence.[29–31] Protamine was selected as an ideal media to transfer heparin information into the DNA amplification signal, since protamine not only forms a strong protamine/DNA complex, but binds even more strongly to heparin through an electrostatic interaction. This is due to the higher charge density (positive charges/mass) and the nearly ideal ion pairing between arginine guanidinium group and heparin's sulfo group.[32] We designed a structure-switchable dumbbell-shaped probe (or dumbbell probe) that contained an intra-strand duplex domain known to be rigid and stable. This dumbbell probe acts as both the response element for strand displacement and the template for the subsequent RCA. In the absence of heparin, the inducing DNA (or i-DNA) is tightly locked by protamine. Owing to the resistance of the dumbbell probe's stabilized stem structure, it remains stable and 'closed' for RCA, resulting in no amplification. When target heparin is introduced, i-DNA is released from protamine and further activates the dumbbell probe to convert into its circular form. This is ascribed to the fact that protamine prefers to bind to heparin instead of DNA due to the stronger affinity of heparin for protamine. After activation, RCA is initiated and the i-DNA is extended from its 3′ terminus by phi29 DNA polymerase, thereby generating hundreds of tandem repeats. The resulting RCA products contain large amounts of stem duplex domain, which can specifically bind with dsDNA-intercalating dye (Sybr Green I) and give a marked increase in fluorescence. Thus, heparin concentration can be sensitively detected based on the change fluorescent intensity.

RCA-blocking effect resulting from protamine

Protamine binds with ssDNA through electrostatic interaction between guanidinium and phosphate groups. Complementary ssDNA hybridize through Watson–Crick base pairing. Thus, there is a competitive relationship between protamine and complementary ssDNA. We hypothesized that protamine could efficiently lock i-DNA blocking the RCA process. We chose a fluorescent reporting platform to investigate this competitive interaction. In the absence of protamine, i-DNA was able to function as a regular primer for opening up the dumbbell probe, as can be seen by the appearance of the strong fluorescence emission around 532 nm (Fig. 2B, curve a). In comparison, addition of protamine disrupts the RCA reaction, and the fluorescence signal gradually fades (Fig. 2B, curve b and c). This observation strongly suggests that protamine and i-DNA formed a sufficiently stable complex to prevent the initiation of the RCA process.

Heparin monitoring behavior

Next, we examined the possibility of exploiting RCA-blocking for heparin sensing. Protamine binds to i-DNA and arrests the RCA reaction (Fig. 3, curve b). When the RCA reaction is carried out in the absence of heparin, the fluorescent intensities are similar to the background signals (Fig. 3, curve a). In contrast, the fluorescent response increased significantly when heparin was introduced (Fig. 3, curve c). The F/F_0 values, obtained under these two situations (Fig. 3 inset $A = F_c/F_0$, inset $B = F_b/F_0$ at 535 nm, F_0 is the fluorescence intensity of the blank) exhibit nearly 36-fold difference. The main reason for this change in fluorescent intensity is the stronger affinity between heparin and protamine. As a result, under the same reaction condition, i-DNA is released from protamine through heparin competition, further initiating the RCA process. The different affinities of heparin and DNA with protamine lead to the major differences in the fluorescence signals. These results suggest that an accurate and rapid heparin measurement can be obtained using an RCA-based sensing platform.

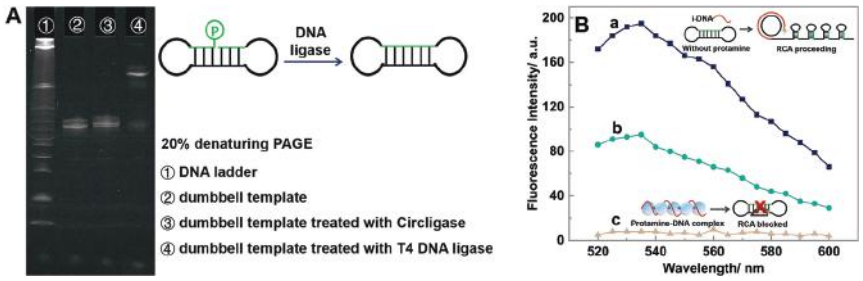

Fig. 2 (A) PAGE analysis of the dumbbell template. (B) Fluorescence spectra of i-DNA induced RCA reaction with different amounts of protamine (a to c: 0, 0.05, 0.1 μg mL^{-1}) in the reaction buffer. The concentrations of i-DNA, dumbbell template, and phi29 DNA polymerase were 10 nM, 10 nM, and 0.05 U μL^{-1}, respectively.

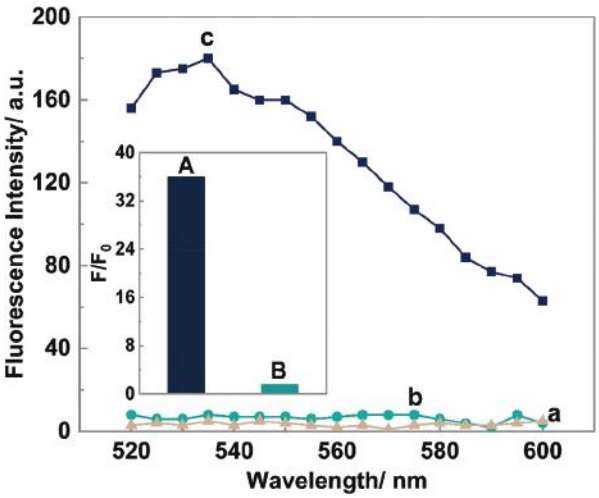

Fig. 3 Fluorescence spectra of (a) system blank and i-DNA induced RCA reaction (b) without and (c) with heparin. The concentrations of i-DNA, dumbbell template, protamine and phi29 DNA polymerase were 10 nM, 10 nM, 0.1 μg mL^{-1} and 0.05 U μL^{-1}, respectively.

Optimization of assay conditions

We studied the impact of five main factors on sensor response to improve the heparin detection performance. The concentration of i-DNA is a crucial parameter for the RCA process. While insufficient i-DNA cannot trigger an effective RCA reaction, when excess i-DNA was used more protamine was required. Fluorescence intensities increased gradually with the growing concentrations of i-DNA (Fig. 4A). A good signal-to-noise ratio was achieved when the i-DNA concentration reached 10 nM. Considering the senor sensitivity, we chose 10 nM as the optimal i-DNA concentration. Protamine binds with i-DNA and functions as the RCA reaction blocker, thus, its amount has a strong influence on the efficiency of amplification reaction. When the protamine concentration was increased, the fluorescence intensity gradually reduced reaching a minimum when the protamine concentration reached 0.1 ng μL^{-1}, indicating the complete prevention of the RCA process (Fig. 4B). Accordingly, the optimal protamine concentration chosen was 0.1 μg mL^{-1}. In addition, the other three important parameters, the RCA reaction time, concentration of reaction buffer, and concentration of dNTP were also optimized in our assay. The dNTP concentration, RCA reaction time and reaction buffer were optimal at 0.25 mM, 60 min and 0.5× in these experiments, respectively (Fig. 4C, D and E).

Fluorescence measurement of heparin

Next we investigated the feasibility of applying RCA-based detection for the quantitative analysis of heparin. Different concentrations of heparin were used and RCA-based detection was applied based on the optimal assay conditions. Measurements were performed three times for each test, and the results are presented in Fig. 5A. We observed that fluorescence gradually increased with the increasing heparin concentrations from 12.5 to 200 ng mL^{-1}. The dependence of the fluorescent value on the heparin concentration is shown in Fig. 5B. An empirical correlation was obtained between fluorescence intensity and the log heparin concentration, as described by: $F = 130.7 - 119.9 \log c$ with a correlation coefficient of $R^2 = 0.984$ (where F is the fluorescence intensity and $\log c$ is the logarithm of the heparin concentration). The detection limit for heparin was 12.5 ng mL^{-1} (0.83 nM) at a signal-to-noise ratio of 3. This concentration is much lower than the therapeutic level of heparin in cardiovascular surgery (2–8 U mL^{-1}, 17–67 μM), postoperative and long-term treatments (0.2–1.2 U mL^{-1}, 1.7–10 μM).[11] These results suggest that ultrasensitive analysis of heparin can be achieved over a wide concentration range through this RCA-based sensing platform.

Finally, to assess the feasibility of the RCA-based sensing platform for heparin detection in complex matrixes, we applied it to analyze spiked heparin in three individual human plasma samples. All the samples were determined by the standard additive recovery method and the target amount found in the different samples were summarized in Table 1. As can be seen, for targets with a concentration falling in the detection dynamic range of the sensor, the recovery ratios of the spiked heparin in three different human plasma samples ranged from 93% to 107% with the relative standard deviation (R.S.D.) less than 6%. These results indicate that the as-proposed RCA-

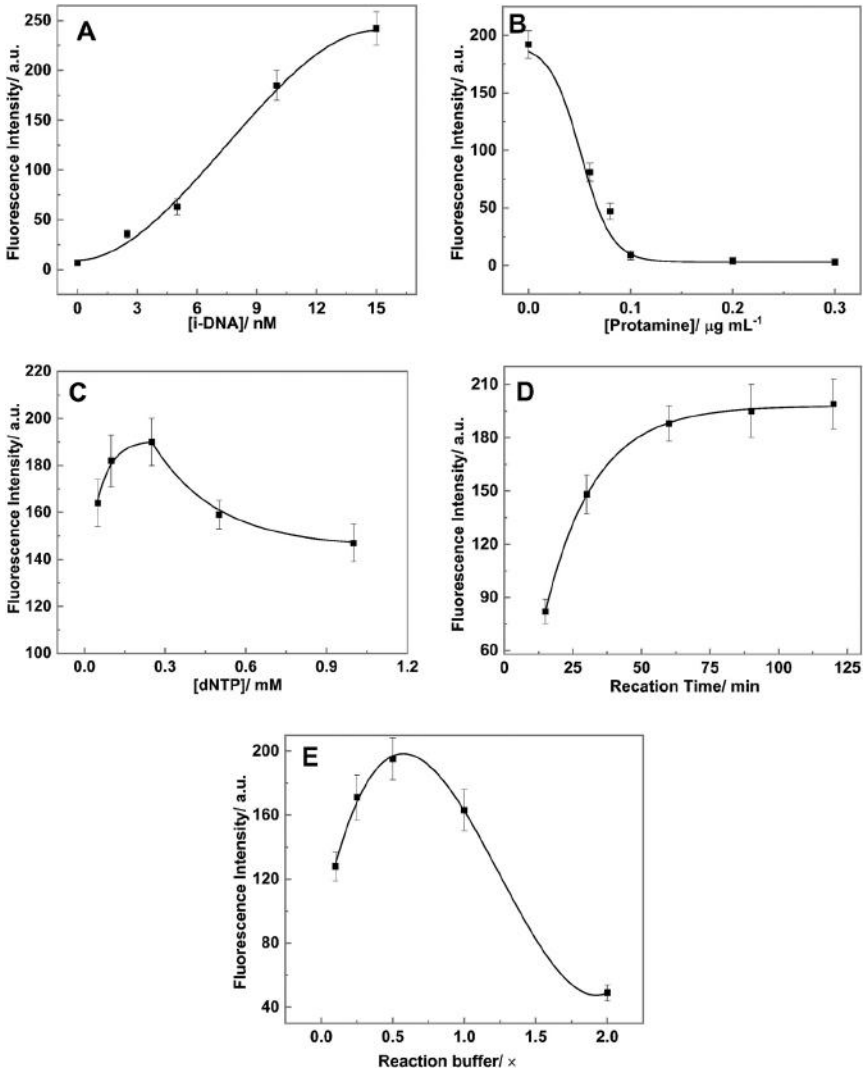

Fig. 4 Optimization of the concentration of (A) i-DNA, (B) protamine concentration, (C) dNTP, (D) RCA reaction time and (E) reaction buffer.

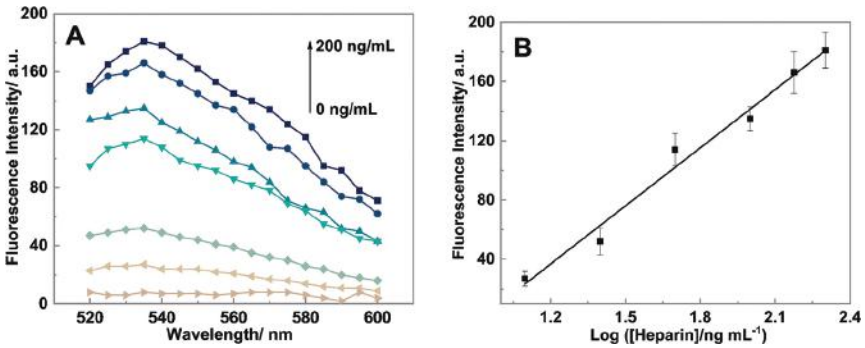

Fig. 5 (A) Fluorescence intensity-wavelength curves with different heparin concentration (bottom to top: 0, 12.5, 25, 50, 100, 150, 200 ng mL^{-1}). (B) Dependence of fluorescence intensity on the logarithm of heparin concentration.

Table 1 Recovery of spiked heparin in human plasma samples

Plasma samples	Added (ng mL^{-1})	Found (ng mL^{-1})	Recovery (%)	R.S.D (%, n = 3)
1	100	107.1	107.1	5.69
	150	156.4	104.3	4.77
	200	213.5	106.8	4.83
2	100	95.2	95.2	2.31
	150	139.6	93.1	3.85
	200	195.2	97.6	3.02
3	100	104.7	104.7	5.56
	150	140.8	93.9	5.79
	200	209.9	105.0	4.24

based biosensor not only exhibits satisfactory accuracy and recovery rate, but also holds great potential for on-site heparin monitoring in complex biological samples because of its robustness, cost efficiency, and highly sensitivity.

Conclusions

We developed an analytical method using a dumbbell probe for the ultrasensitive, isothermal detection of heparin relying on its unique interaction with protamine using a rolling circle technique for signal amplification. This method works over a wide linear range and exhibits a detection limit for heparin of 12.5 ng mL^{-1} (0.83 nM). This concentration is much lower than the therapeutic level of heparin in cardiovascular surgery (17–67 μM) and in postoperative and long-term treatment (1.7–10 μM). The application of this assay may avoid complications induced by heparin overdose. This method offers three major advantages: (1) by taking advantage of rolling circle amplification, the LOD is improved significantly; (2) the method is simple and inexpensive, as it does not rely on expensive instruments; and (3) the specificity of heparin recognition is high as random nucleic acids cannot activate dumbbell-shaped structure. Given the crucial roles of heparin, this new method can greatly facilitate clinical diagnosis and improve our understanding of the biological roles of heparin.

Live subject statement

All experiments were performed in accordance with the International Ethical Guidelines for Biomedical Research Involving Human Subjects of World Health Organization, and approved by the ethics committee at Nanjing Normal University (IRB-202003002). The blood samples were gathered from healthy volunteers in Nanjing Hospital of Chinese Medicines and informed consents were obtained from human participants of this study.

Conflicts of interest

There are no conflicts to declare.

Acknowledgements

This work was supported by grants from National Natural Science Foundation, China (22006070 to L. L.), National Institutes of Health (DK111958 and CA231074 to R. J. L.), Natural Science Foundation of Jiangsu Province (BK20200718 to B. L.), and Natural Science Research Project of Jiangsu Higher Education Institutions (19KJB150012 to L. L.).

References

1 M. E. Meyerhoff, V. C. Yang, J. A. Wahr, L. M. Lee, J. H. Yun, B. Fu and E. Bakker, *Clin. Chem.*, 1995, **41**, 1355–1356.
2 R. J. Linhardt, *J. Med. Chem.*, 2003, **46**, 2551–2564.
3 J. Liu and R. J. Linhardt, *Nat. Prod. Rep.*, 2014, **31**, 1676–1685.
4 E. I. Oduah, R. J. Linhardt and S. T. Sharfstein, *Pharmaceuticals*, 2016, **9**, 38.
5 I. Bhushan, A. Alabbas, J. C. Sistla, R. Saraswat, U. R. Desai and R. B. Gupta, *Int. J. Biol. Macromol.*, 2017, **99**, 721–730.
6 V. Šuštar, R. Janša, M. Frank, H. Hagerstrand, M. Kržan, A. Iglič and V. Kralj-Iglič, *Blood Cells, Mol., Dis.*, 2009, **42**, 223–227.
7 J. M. Choi, V. Bourassa, K. Hong, M. Shoga, E. Y. Lim, A. Park, K. Apaydin and A. K. Udit, *Mol. Pharmaceutics*, 2018, **15**, 2997–3004.
8 X. M. Wu, F. Zhang and Y. Li, *J. Mater. Chem. B*, 2018, **6**, 5466–5475.
9 T. E. Warkentin, M. N. Levine, J. Hirsh, P. Horsewood, R. S. Roberts, M. Gent and J. G. Kelton, *N. Engl. J. Med.*, 1995, **332**, 1330–1336.
10 G. J. Despotis, G. Gravlee, K. Filos, J. Levy and D. M. Fisher, *Anesthesiology*, 1999, **91**, 1122–1151.
11 B. Girolami and A. Girolami, *Semin. Thromb. Hemostasis*, 2006, **32**, 803–809.
12 R. Zhan, Z. Fang and B. Liu, *Anal. Chem.*, 2010, **82**, 1326–1333.
13 D. J. Murray, W. J. Brosnahan, B. Pennell, D. Kapalanski, J. M. Weiler and J. Olson, *J. Cardiothorac. Vasc. Anesth.*, 1997, **11**, 24–28.
14 P. D. Raymond, M. J. Ray, S. N. Callen and N. A. Marsh, *Perfusion*, 2003, **18**, 269–276.
15 M. N. Levine, J. Hirsh, M. Gent, A. G. Turpie, M. Cruickshank, J. Weitz, D. Anderson and M. Johnson, *Arch. Intern. Med.*, 1994, **154**, 49–56.
16 M. E. Meyerhoff, B. Fu, E. Bakker, J. H. Yun and V. C. Yang, *Anal. Chem.*, 1996, **68**, 168A–175A.
17 N. Ramamurthy, N. Baliga, J. A. Wahr, U. Schaller, V. C. Yang and M. E. Meyerhoff, *Clin. Chem.*, 1998, **44**, 606–613.
18 H. Qi, L. Zhang, L. Yang, P. Yu and L. Mao, *Anal. Chem.*, 2013, **85**, 3439–3445.
19 H. Groult, N. Poupard, F. Herranz, E. Conforto, N. Bridiau, F. Sannier, S. Bordenave, J.-M. Piot, J. Ruiz-Cabello,

I. Fruitier-Arnaudin and T. Maugard, *Biomacromolecules*, 2017, **18**, 3156–3167.
20 X. Zhang, X. Han, K. Xia, Y. Xu, Y. Yang, K. Oshima, S. M. Haeger, M. J. Perez, S. A. McMurtry, J. A. Hippensteel, J. A. Ford, P. S. Herson, J. Liu, E. P. Schmidt and R. J. Linhardt, *Proc. Natl. Acad. Sci. U. S. A.*, 2019, **116**, 9208–9213.
21 G. W. Hart and R. J. Copeland, *Cell*, 2010, **143**, 672–676.
22 K. Mariño, J. Bones, J. J. Kattla and P. M. Rudd, *Nat. Chem. Biol.*, 2010, **6**, 713–723.
23 J. C. Paulson, O. Blixt and B. E. Collins, *Nat. Chem. Biol.*, 2006, **2**, 238–248.
24 J. Zaia, *OMICS*, 2010, **14**, 401–418.
25 M. G. Mohsen and E. T. Kool, *Acc. Chem. Res.*, 2016, **49**, 2540–2550.
26 M. M. Ali, F. Li, Z. Zhang, K. Zhang, D. K. Kang, J. A. Ankrum, X. C. Le and W. Zhao, *Chem. Soc. Rev.*, 2014, **43**, 3324–3341.
27 C. C. Chang, C. C. Chen, S. C. Wei, H. H. Lu, Y. H. Liang and C. W. Lin, *Sensors*, 2012, **12**, 8319–8337.
28 Y. Zhou, Q. Huang, J. Gao, J. Lu, X. Shen and C. Fan, *Nucleic Acids Res.*, 2010, **38**, e156.
29 A. Shvarev and E. Bakker, *J. Am. Chem. Soc.*, 2003, **125**, 11192–11193.
30 L. Wang, F. Shi, Y. Li and X. Su, *Sens. Actuators, B*, 2016, **222**, 945–951.
31 Z. Zhou and S. Dong, *Nanoscale*, 2015, **7**, 1296–1300.
32 J. R. Fromm, R. E. Hileman, E. E. O. Caldwell, J. M. Weiler and R. J. Linhardt, *Arch. Biochem. Biophys.*, 1995, **323**, 279–287.

